

# Sensitivity and pointing accuracy of the NEMO km<sup>3</sup> telescope

C. Distefano <sup>a</sup> for the NEMO Collaboration

<sup>a</sup>*Laboratori Nazionali del Sud, INFN, Catania, Italy*

---

## Abstract

In this paper we present the results of Monte Carlo simulation studies on the capability of the proposed NEMO km<sup>3</sup> telescope to detect high energy neutrinos. We calculated the detector sensitivity to muon neutrinos coming from a generic point-like source. We also simulated the lack of atmospheric muons in correspondence to the Moon disk in order to determine the detector angular resolution and to check the absolute pointing capability.

*Key words:* Point sources, Neutrino telescopes, NEMO

*PACS:* 95.55.Vj, 95.85.Ry, 96.40.Tv

---

## 1. Introduction

The NEMO Collaboration is conducting an R&D activity towards the construction of a Mediterranean km<sup>3</sup> neutrino telescope [1]. In this work, we present a first study of the expected response of the proposed NEMO km<sup>3</sup> detector to neutrinos from point-like sources. In section 2, we describe the generation of the atmospheric neutrinos and muons background. We define the detector sensitivity and the event selection criteria. Eventually, we determine the detector sensitivity to a muon neutrino flux from a generic point-like source. In section 3, we present results on possible Moon shadow detection. We then estimate the detector angular resolution and we check the effects of errors in the detector absolute orientation in the pointing accuracy.

The geometry of the km<sup>3</sup> telescope, simulated in this work, is the NEMOdh-140 described in [2]. The detector response is simulated using the ANTARES simulation codes [3], taken into account the water optical parameters measured in the site of Capo Passero [4].

## 2. Detector sensitivity to point-like sources

The detector sensitivity is here calculated following the the Feldman & Cousins approach [5]. In particular we define the sensitivity as:

$$\left( \frac{d\varphi_\nu}{d\varepsilon_\nu} \right)_{90} = \frac{\overline{\mu}_{90}(b)}{n_s} \left( \frac{d\varphi_\nu}{d\varepsilon_\nu} \right)_0, \quad (1)$$

where  $\overline{\mu}_{90}(b)$  is the 90% c.l. average upper limit for an expected background with *known* mean  $b$  and  $(d\varphi_\nu/d\varepsilon_\nu)_0$  is an arbitrary source spectrum predicting a mean signal  $n_s$ .

---

*Email address:* carla.distefano@lns.infn.it (C. Distefano).

## 2.1. Simulation of the atmospheric background

A sample of  $7 \cdot 10^9$  atmospheric neutrinos have been generated using the ANTARES generation code, in the energy range  $10^2 \div 10^8$  GeV, with a spectral index  $X=2$  and a  $4\pi$  isotropic angular distribution. The events are weighted to the sum of the Bartol flux [6] and of prompt neutrino **rqpm** model [7] flux. Atmospheric muons are generated at the detector, applying a weighted generation technique. We simulated  $5.5 \cdot 10^7$  events in the energy range  $10^2 \div 10^6$  GeV. The events are weighted to the Okada parameterization [8], taking into account the depth of the Capo Passero site ( $D = 3500$  m) and the flux variation inside the detector sensitive height.

## 2.2. Criteria for atmospheric events rejection

The used reconstruction algorithm is a robust track fitting procedure based on a maximization likelihood method. We use, as *goodness of fit* criterion, the variable:

$$\Lambda \equiv -\frac{\log(\mathcal{L})}{N_{DOF}} + 0.1(N_{comp} - 1), \quad (2)$$

where  $\log(\mathcal{L})/N_{DOF}$  is the log-likelihood per degree of freedom and  $N_{comp}$  is the total number of  $1^\circ$  compatible solutions [3]. A quality cut  $\Lambda > \Lambda_{cut}$  is applied together with other selection criteria: the muon must be reconstructed as up-going; the event must be reconstructed with a number of hits  $N_{fit} > N_{fit}^{cut}$ ; only events reconstructed in a circular sky region centered in the source position and having a radius of  $r_{bin}$  are considered. The optimal values of  $\Lambda_{cut}$ ,  $N_{fit}^{cut}$  and  $r_{bin}$  are chosen to minimize the detector sensitivity, taking into account both atmospheric neutrino and muon background.

## 2.3. Sensitivity to a generic point-like source

We simulated muons induced by  $\sim 10^9$  neutrinos with energy range  $10^2 \div 10^8$  GeV and  $X=1$ . These events are weighted to the neutrino spectrum  $(d\varphi_\nu/d\varepsilon_\nu)_0 = 10^{-7}\varepsilon_{\nu, GeV}^{-\alpha}$  ( $\text{GeV}^{-1} \text{cm}^{-2} \text{s}^{-1}$ ). As a representative case, the source position is chosen at a declination of  $\delta = -60^\circ$ . In Table

1, we report the expected sensitivity for different spectral index  $\alpha$ , compared to the IceCube telescope [9]. In Fig. 1 we plot the NEMO sensitivity for  $\alpha = 2$  as a function of years of data taking, compared to the IceCube sensitivity obtained for a  $1^\circ$  search bin [9]. The proposed NEMO detector shows a better sensitivity to muon neutrino fluxes, reached in a smaller search bin.

NEMO							IceCube
$\alpha$	$\Lambda_{cut}$	$N_{fit}^{cut}$	$r_{bin}$	$\bar{\mu}_{90}(b)$	$\varepsilon_\nu^\alpha (d\varphi_\nu/d\varepsilon_\nu)_{90}$	$\varepsilon_\nu^\alpha (d\varphi_\nu/d\varepsilon_\nu)_{90}$	
1.0	7.6	26	0.4°	2.43	$1.9 \cdot 10^{-15}$	$2.4 \cdot 10^{-15}$	
1.5	7.3	-	0.5°	2.45	$2.6 \cdot 10^{-12}$	$4.5 \cdot 10^{-12}$	
2.0	7.3	-	0.5°	2.45	$1.2 \cdot 10^{-9}$	$2.4 \cdot 10^{-9}$	
2.5	7.3	-	0.6°	2.48	$2.3 \cdot 10^{-7}$	$3.8 \cdot 10^{-5}$	

Table 1

Sensitivity to a point-like neutrino source at  $\delta = -60^\circ$ , for different spectral indexes  $\alpha$  and 3 years of data taking, and comparison with the IceCube detector [9]. The sensitivity spectrum  $\varepsilon_\nu^\alpha (d\varphi_\nu/d\varepsilon_\nu)_{90}$  is expressed in  $\text{GeV}^{\alpha-1} / \text{cm}^2 \text{s}$ .

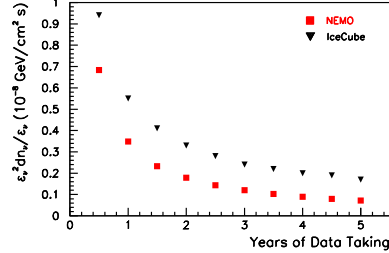


Fig. 1. Sensitivity to a neutrino spectrum with  $\alpha = 2$ , coming from a  $\delta = -60^\circ$  declination point-like source and comparison with the IceCube detector [9].

## 3. Detection of the Moon shadow

Since the Moon absorbs cosmic rays, we expect a lack of atmospheric muons from the direction of the Moon disk (angular radius  $R_{Moon} = 0.26^\circ$ ). The detection of this muon deficit, commonly called *Moon shadow*, provides a measurement of the detector angular resolution; besides detecting its position in the sky allows us to determine the absolute orientation of the detector [10]. In this section, we present first results of our Monte Carlo simulations.

### 3.1. Simulation of atmospheric muons

Atmospheric muons are generated as described in section 2.1, we implemented the calculation of the Moon position to simulate the muon lack. We simulated  $1.25 \cdot 10^8$  events in the energy range  $10^2 \div 10^6$  GeV, restricting the generation in a circular window around the Moon position with a radius of  $10^\circ$ . The events are then weighted to the Okada parameterization.

### 3.2. Estimate of the detector angular resolution

The number  $N_\mu$  of muons reconstructed within a distance  $D$  from the Moon centre is plotted in Fig. 2. The distribution is then fitted using the function:

$$\frac{dN_\mu}{dD^2} = k \left( 1 - \frac{R_{Moon}^2}{2\sigma^2} \exp\left(\frac{D^2}{2\sigma^2}\right) \right), \quad (3)$$

obtaining from the fit an angular resolution  $\sigma = 0.19^\circ \pm 0.2^\circ$ . During the fit procedure, we apply an event selection imposing  $\Lambda_{cut} = -7.6$  and  $N_{fit}^{min} = 20$ , reaching, in this way, a detection significance  $S_{1\text{yr}} \sim 5.3$  in 1 year of data taking. Assuming a required significance of 3, the minimum time needed to observe the shadow is therefore of the order of 100 days.

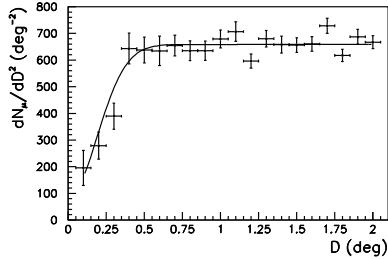


Fig. 2. Selected muon event density versus the angular distance from the Moon centre. The line represents the result of the fit in Eq.(3), obtained for  $k = (659 \pm 8) \text{ deg}^{-2}$  and  $\sigma = 0.19^\circ \pm 0.2^\circ$ .

### 3.3. Check of the detector pointing accuracy

Up to now, we assumed to well know the detector absolute orientation. The effect of a possible error in the absolute azimuthal orientation is here

simulated, introducing a rotation  $\Psi$  in the reconstructed tracks around the Z axis. In Fig. 3, we plot the selected events in a 2D celestial map referring to the Moon position, for  $\Psi = 0^\circ, 0.2^\circ, 0.4^\circ$  and  $0.6^\circ$ . For the expected accuracy  $\Psi \leq 0.2^\circ$ , the shadow is still observable at the Moon position, while considering the pessimistic case  $\Psi \geq 0.2^\circ$ , systematic errors may be corrected. A detailed study together with the effects of errors in the absolute zenithal orientation are still under analysis.

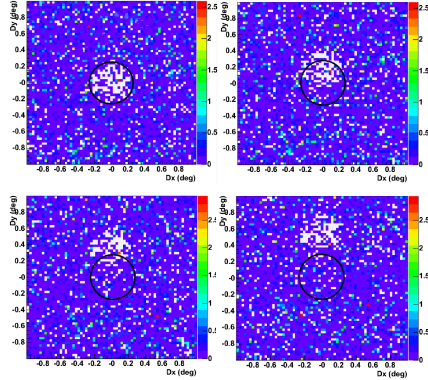


Fig. 3. Celestial map of selected events, referring to the Moon position, for  $\Psi = 0^\circ$  (top-left),  $0.2^\circ$  (top-right),  $0.4^\circ$  (bottom-left) and  $0.6^\circ$  (bottom-right). The black circle represents the Moon disk.

## References

- [1] E. Migneco for the NEMO Collaboration, proc. in this workshop. The NEMO web site: nemoweb.lns.infn.it.
- [2] R. Coniglione for the NEMO Collaboration, proc. in this workshop.
- [3] Y. Becherini for the ANTARES Collaboration, proc. in this workshop.
- [4] The NEMO Collaboration, *Study and characterization of a deep sea site for a km3 underwater neutrino telescope*, report to ApPEC (2002).
- [5] G.J. Feldman & R.D. Cousins, Phys. Rev. D57 (1998) 3873.
- [6] V. Agrawal et al., Phys. Rev. D53 (1996) 1314.
- [7] E.V. Bugaev, Phys. Rev. D58 (1998) 054001.
- [8] A. Okada, Astrop. Phys. 2 (1994) 393.

- [9] J. Ahrens et al., *Astropart. Phys.* 20 (2004) 507.
- [10] M. Ambrosio et al., *Astropart. Phys.* 20 (2003) 145.